



**Original Research Article**

**A DFT Outlook on Bupropion Adsorption on the Surface of C<sub>8</sub>B<sub>6</sub>N<sub>6</sub> Nanocluster**

**Mohammad Hossein Razeghi<sup>1,\*</sup>, Ozra Gholipour<sup>2</sup>, Simin Arabi<sup>3</sup>, Ebrahim Nemati-Kande<sup>4</sup>, Jaber Jahanbin Sardroodi<sup>1,\*</sup>**

<sup>1,\*</sup> Department of Chemistry, Azarbaijan Shahid Madani University, Tabriz, Iran.

<sup>2</sup> Department of applied Chemistry, Chemistry faculty, Urmia university, Urmia, Iran.

<sup>3</sup> Department of Chemistry, Shahr-e-Qods Branch, Islamic Azad University, Tehran, Iran

<sup>4</sup> Department of Physical Chemistry, Chemistry faculty, Urmia University, Urmia, Iran.

*Received: 2025-02-04*

*Accepted: 2025-04-06*

*Published: 2025-04-07*

**ABSTRACT**

This study investigated the effectiveness of the C<sub>8</sub>B<sub>6</sub>N<sub>6</sub> nanocluster as an adsorbent and sensor for the removal and detection of bupropion (BP) using density functional theory (DFT) methods. The results indicated that while BP interaction with C<sub>8</sub>B<sub>6</sub>N<sub>6</sub> nanocage is experimentally feasible, the interactions have a reversible semi-chemisorption nature. The thermodynamic analysis revealed that the adsorption process is exothermic and spontaneous, as evidenced by the negative values of  $\Delta H_{ad}$  and  $\Delta G_{ad}$ . Temperature and solvent effects were also assessed, showing that adsorption is more effective at lower temperatures and in the absence of water, i.e., in the gas phase. In terms of electronic properties, the C<sub>8</sub>B<sub>6</sub>N<sub>6</sub> nanocage exhibited a 52% reduction in its bandgap, decreasing from 2.380 eV to 1.144 eV upon interaction with BP. These findings suggest that the C<sub>8</sub>B<sub>6</sub>N<sub>6</sub> nanocluster not only exhibits superior adsorption efficiency for BP removal but also demonstrates enhanced suitability as a sensing material for the electrochemical detection of BP.

**Keywords:** Fullerene, Bupropion, Adsorption, Density functional theory, Adsorptive removal, Sensor

\*Corresponding author email address: [jsardroodi@azaruniv.edu](mailto:jsardroodi@azaruniv.edu), [M.h.razeghi@azaruniv.ac.ir](mailto:M.h.razeghi@azaruniv.ac.ir)

## Introduction

The occurrence of pharmaceutical compounds in the environment has become an emerging concern due to their widespread use and improper disposal [1]. These compounds, including antibiotics, analgesics, hormones, and especially antidepressants, are introduced into water bodies and soil through various pathways such as wastewater discharge, agricultural runoff, and landfill leachate [2-4]. Many wastewater treatment plants are not equipped to fully remove these substances, allowing them to persist in the environment at trace levels. The presence of pharmaceuticals in ecosystems poses several disadvantages [5]. They can disrupt aquatic life by interfering with the hormonal systems of fish and other organisms, leading to reproductive and developmental abnormalities [6]. Additionally, the proliferation of antibiotic residues in the environment contributes to the alarming rise of antibiotic-resistant bacteria, which poses a significant public health threat [7]. Furthermore, the long-term effects of chronic exposure to low concentrations of these compounds on both wildlife and humans remain poorly understood, raising concerns about potential toxicity and bioaccumulation [8]. Bupropion (BP, Figure 1) is an atypical antidepressant commonly prescribed for major depressive disorder, seasonal affective disorder, and smoking cessation [9-11]. While generally well-tolerated, BP toxicity can occur due to overdose or interactions with other substances, leading to serious clinical manifestations [12]. Symptoms of toxicity may include seizures, tachycardia, hypertension, hallucinations, agitation, and, in severe cases, cardiac arrhythmias or loss of consciousness [13]. Common side effects of bupropion at therapeutic doses include insomnia, dry mouth, headache, dizziness, and gastrointestinal disturbances [14]. Rare but significant adverse effects include an increased risk of seizures, particularly in individuals with predisposing factors such as a history of seizures, eating disorders, or concurrent use of other medications that lower the seizure threshold [15]. Therefore, Determination and removal of BP is of great importance. Analytical methods such as high-performance liquid chromatography (HPLC), gas chromatography-mass spectrometry (GC-MS), and liquid chromatography-tandem mass spectrometry (LC-MS/MS) are commonly employed for the measurement of BP [16-19]. However, the preferred techniques suffer from several downsides including being expensive, time-consuming, requiring sophisticated operators for the implementation of sample pre-treatment steps, and consuming organic solvents [16]. On the other hand, electrochemical sensors are portable and economical analytical tools that can be a good alternative to the mentioned techniques because of their simplicity, rapid analysis

procedure, and being environmentally friendly [17]. Besides, adsorption offers several advantages over other removal techniques for eliminating pharmaceutical compounds from the environment [18]. One of its primary benefits is its high efficiency and effectiveness in removing a wide range of contaminants, even at low concentrations, which is particularly important given the trace levels at which pharmaceuticals often persist in water sources [19]. Unlike advanced oxidation processes or membrane filtration, adsorption typically requires lower energy inputs, making it a more cost-effective and environmentally friendly solution [20]. Additionally, the use of adsorbents such as nanostructures allows for flexibility in application and adaptability to different water matrices. Adsorption systems are relatively simple to operate and maintain, often requiring less technical expertise compared to complex chemical or biological methods [21]. Furthermore, adsorption does not produce harmful byproducts or residues, as some chemical treatments might, reducing the risk of secondary pollution [20]. These advantages make adsorption a promising and sustainable approach for mitigating the environmental impact of pharmaceutical contaminants [19].

The  $C_8B_6N_6$  nanocluster (Figure 1) is a highly promising material in the fields of adsorption and sensing due to its unique structural, electronic, and chemical properties. Composed of carbon (C), boron (B), and nitrogen (N) atoms, this nanocluster exhibits exceptional stability and a well-defined geometry, which contribute to its high surface area and abundant active sites [22]. The presence of boron and nitrogen atoms introduces a significant degree of polarity and electron density modulation, enhancing its ability to interact with a wide range of chemical species through mechanisms such as hydrogen bonding, van der Waals forces, and  $\pi$ - $\pi$  interactions [23]. Additionally, the electronic configuration of the  $C_8B_6N_6$  nanocluster enables strong adsorption of target molecules while maintaining selectivity, making it particularly effective for detecting gases, organic compounds, and environmental pollutants [24]. Its nanoscale size further ensures rapid response times and high sensitivity in sensor applications. Moreover, the non-toxic and environmentally friendly nature of its constituent elements makes it a sustainable choice for practical applications [25]. These attributes collectively position the  $C_8B_6N_6$  nanocluster as a versatile and efficient material for use in advanced adsorption systems and highly sensitive chemical sensors [25]. In this respect, the performance of  $C_8B_6N_6$  fullerene as an adsorbent and

sensor for the adsorptive removal and detection of BP was investigated by density functional theory (DFT) computations, for the first time, in this research.

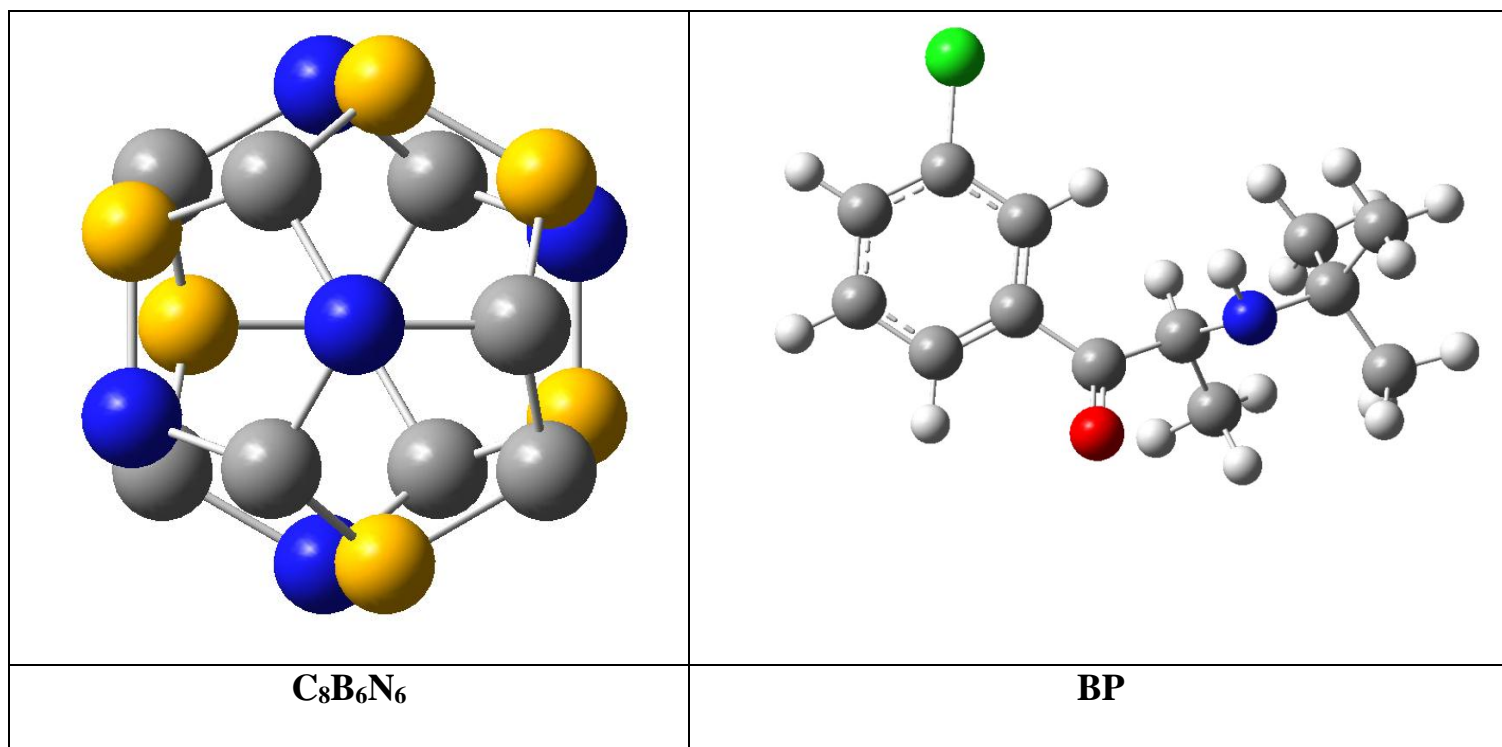


**Figure 1.** The optimized structures of BP and C<sub>8</sub>B<sub>6</sub>N<sub>6</sub> (grey: carbon, white: hydrogen, red: oxygen, blue: nitrogen, yellow: boron, green: chlorine)

### Computational Methods

The structural configurations of boron phosphide (BP), C<sub>8</sub>B<sub>6</sub>N<sub>6</sub>, and their diverse combinations were meticulously designed and thoroughly examined using advanced computational tools, specifically GaussView 6 [26] in conjunction with Nanotube Modeler 1.3.0.3 [27]. These software platforms facilitated the precise modeling and visualization of the nanostructures, enabling an in-depth exploration of their intricate molecular geometries. The initial phase of the study involved performing rigorous geometric optimization for each individual structure to ensure their stability and confirm their suitability for further analyses. This critical step served as the foundation for generating accurate, reliable, and meaningful computational data. Following the optimization process, a comprehensive suite of computational evaluations was undertaken to probe the electronic and structural properties of the studied systems. Among these evaluations,

infrared (IR) spectroscopy was employed to investigate vibrational modes and bonding characteristics, while frontier molecular orbital (FMO) analyses provided insights into the electronic behavior, including the distribution of the highest occupied molecular orbital (HOMO) and lowest unoccupied molecular orbital (LUMO). These analyses shed light on the electronic transitions and bonding interactions within the nanostructures. To ensure precision and reliability in these computational studies, density functional theory (DFT) was utilized as the primary theoretical framework. Specifically, the B3LYP functional combined with the 6-31G(d) basis set was chosen for its proven accuracy in modeling molecular systems. All calculations were performed using the Gaussian 16 software package [28], which is renowned for its robust capabilities in quantum chemical computations. This methodological approach enabled a detailed exploration of the molecular dynamics, electronic structures, and bonding features of these complex nanomaterials. The integration of advanced computational techniques with high-level theoretical methods allowed for a profound understanding of the fundamental properties and potential applications of BP, C<sub>8</sub>B<sub>6</sub>N<sub>6</sub>, and their hybrid configurations. Through this meticulous and systematic investigation, valuable insights were gained into the behavior of these nanostructures, paving the way for future research in the field of nanoscale materials science. The study employed this theoretical framework due to its widespread credibility among scientists and its strong consistency with experimental data. Known for its reliability in forecasting experimental behavior, this methodology ensured that computational findings mirrored real-world scenarios. In this study, a series of computational simulations were meticulously carried out to explore the adsorption behavior of drugs under varying conditions, with particular attention given to both gaseous and liquid phases. These simulations employed the Conductor-like Polarizable Continuum Model (CPCM), a widely recognized theoretical framework designed to account for the effects of solvation on molecular systems. By incorporating CPCM, the study was able to simulate the interactions between solute and solvent molecules, thereby providing a more accurate representation of real-world conditions. The temperature range investigated spanned from 298 K to 318 K, enabling a detailed examination of how thermal variations influence the adsorption process. A primary focus was placed on aqueous systems, given their relevance to biological and pharmaceutical applications. The adsorption of drugs onto an adsorbent surface was analyzed with precision, aiming to uncover the intricate relationships between solvation dynamics, temperature changes, and adsorption efficiency. This

comprehensive approach offers valuable insights into the thermodynamic principles that govern drug adsorption processes, particularly in water-based environments. Such findings have significant implications for advancing drug delivery technologies, as they may contribute to the development of more effective and targeted delivery systems. By elucidating these fundamental interactions, the study holds the potential to enhance our understanding of solvation effects and thermal dependencies, ultimately paving the way for innovative strategies in pharmaceutical science. The following process was scrutinized:



Our research undertook an extensive and detailed investigation into the intricate interaction between the drug molecule and the adsorbent material, focusing on the calculation of adsorption energy values ( $E_{\text{ad}}$ ) as well as a comprehensive suite of thermodynamic parameters. These thermodynamic parameters encompassed several critical factors, including the thermodynamic equilibrium constant ( $K_{\text{th}}$ ), the changes in entropy associated with the adsorption process ( $\Delta S_{\text{ad}}$ ), the variations in Gibbs free energy ( $\Delta G_{\text{ad}}$ ), and the shifts observed in adsorption enthalpy ( $\Delta H_{\text{ad}}$ ). To facilitate this thorough analysis, we relied on a robust mathematical framework that utilized a series of equations, specifically equations numbered 2 through 6, which provided a systematic and reliable basis for exploring the thermodynamic characteristics of the adsorption phenomenon. By employing these equations, we were able to delve into the energetic and entropic contributions that underpin the adsorption mechanism, thereby enabling a nuanced understanding of how these factors collectively influence the interaction. This methodological approach allowed us to quantify not only the energetic feasibility but also the thermodynamic efficiency of the drug-adsorbent interaction under varying experimental conditions. The insights gained from this study are invaluable, as they shed light on the fundamental principles governing adsorption processes, offering a deeper understanding of how such interactions can be optimized for practical applications. Consequently, our findings contribute meaningfully to the broader scientific discourse on adsorption mechanisms, providing a strong foundation for future research and potential advancements in related fields [25].

$$E_{\text{ad}} = \left( E_{(\text{BP-C}_8\text{B}_6\text{N}_6)} - \left( E_{(\text{BP})} + E_{(\text{C}_8\text{B}_6\text{N}_6)} + E_{(\text{BSSE})} \right) \right) \quad (2)$$

$$\Delta H_{\text{ad}} = \left( H_{(\text{BP-C}_8\text{B}_6\text{N}_6)} - \left( H_{(\text{BP})} + H_{(\text{C}_8\text{B}_6\text{N}_6)} \right) \right) \quad (3)$$

$$\Delta G_{\text{ad}} = \left( G_{(\text{BP-C8B6N6})} - (G_{(\text{BP})} + G_{(\text{C8B6N6})}) \right) \quad (4)$$

$$\Delta S_{\text{ad}} = \left( S_{(\text{BP-C8B6N6})} - (S_{(\text{BP})} + S_{(\text{C8B6N6})}) \right) \quad (5)$$

$$K_{\text{th}} = \left( \exp - (\Delta G_{\text{ad}}/RT) \right) \quad (6)$$

In the mathematical framework of the equations currently under evaluation, the symbol "E" is employed to represent the total electronic energy that is intrinsically linked to each molecular or structural configuration under consideration. This parameter is crucial as it provides a foundational understanding of the electronic characteristics and stability of the system being studied. Complementing this, the term "E<sub>BSSSE</sub>" denotes the basis set superposition error correction, a critical adjustment applied to counteract inaccuracies arising from the overlap of basis sets in quantum chemical computations. This correction ensures a higher degree of precision in the calculated energy values, which is indispensable for reliable theoretical predictions.

Furthermore, the variable "H" symbolizes the total energy of the system, which is refined by incorporating thermal enthalpy corrections. This adjustment is essential for aligning theoretical energy values with thermodynamic conditions that prevail in experimental setups. Similarly, "G" represents the total energy modified by incorporating the thermal correction of Gibbs free energy, a parameter extensively discussed in scientific literature due to its relevance in predicting spontaneity and equilibrium conditions in chemical processes. In addition to these variables, the constant "R" is introduced, denoting the ideal gas constant, a fundamental physical constant that plays a pivotal role in thermodynamic calculations. The symbol "S" corresponds to the thermal correction entropy, a measure of the disorder or randomness within the system, which is particularly significant for understanding the thermodynamic behavior of the structures under analysis. Finally, "T" is used to indicate the temperature at which these computational evaluations are conducted, as temperature profoundly influences the thermodynamic and kinetic properties of materials. The equations numbered 7 through 12 serve as critical tools for deriving multiple key properties associated with frontier molecular orbitals. These properties include the bandgap ( $E_g$ ), which provides insights into the electronic transitions and conductivity of materials; chemical hardness ( $\eta$ ), a measure of resistance to electronic deformation; chemical

potential ( $\mu$ ), which reflects the tendency of electrons to escape from a system; electrophilicity ( $\omega$ ), an index quantifying the electrophilic nature of a molecule; and the maximum charge transfer capacity ( $\Delta N_{\max}$ ), a parameter that characterizes the extent to which charge can be transferred within or between molecular systems. These properties are indispensable for understanding and predicting the chemical reactivity, stability, and electronic behavior of materials under investigation [23, 24].

$$E_g = E_{\text{LUMO}} - E_{\text{HOMO}} \quad (7)$$

$$\% \Delta E_g = \frac{E_{g2} - E_{g1}}{E_{g1}} \times 100 \quad (8)$$

$$\eta = (E_{\text{LUMO}} - E_{\text{HOMO}}) / 2 \quad (9)$$

$$\mu = (E_{\text{LUMO}} + E_{\text{HOMO}}) / 2 \quad (10)$$

$$\omega = \mu^2 / 2\eta \quad (11)$$

$$\Delta N_{\max} = \mu / \eta \quad (12)$$

Molecular orbital theory serves as a cornerstone for comprehending the electronic properties and behaviors of various materials. At the heart of this theoretical framework lie two critical parameters: ELUMO and EHOMO. ELUMO, an abbreviation for the energy level of the Lowest Unoccupied Molecular Orbital, represents the molecular orbital that is unoccupied yet closest in energy to the occupied orbitals. Conversely, EHOMO, or the energy level of the Highest Occupied Molecular Orbital, refers to the molecular orbital that is fully occupied and possesses the highest energy among such orbitals. These two energy levels, ELUMO and EHOMO, are pivotal in determining a molecule's electronic structure, reactivity, and overall behavior in various chemical and physical contexts. The difference between these two energy levels, often referred to as the bandgap, plays a critical role in defining several key properties of materials. This bandgap, which quantifies the energy required for an electron to transition from the HOMO to the LUMO, is a fundamental determinant of a material's optical and electronic characteristics. Specifically, the magnitude of this bandgap influences how a material interacts with light, thereby shaping its optical absorption spectrum, photoluminescence properties, and overall

optical behavior. Furthermore, the bandgap is intimately connected to a material's electrical conductivity, as it governs the ease with which electrons can be excited from the valence band (associated with HOMO) to the conduction band (associated with LUMO). Materials with small bandgaps typically exhibit higher electrical conductivity due to the relatively low energy barrier for electron excitation, while those with larger bandgaps tend to behave as insulators or semiconductors. In this context, two specific complexes have recently attracted significant attention within the scientific community: the Nano-adsorbent and the BP-Adsorbent. These complexes are being actively studied for their unique electronic properties and potential applications in various fields, including catalysis, environmental remediation, and advanced material design. The respective bandgaps of these complexes denoted as  $E_{g1}$  for the Nano-adsorbent and  $E_{g2}$  for the BP-Adsorbent, are currently under investigation to elucidate their roles in determining the functional characteristics of these materials. These studies aim to provide deeper insights into how variations in bandgap values influence the performance and efficacy of such complexes in practical applications. References [18-20] further elaborate on these findings, underscoring the importance of molecular orbital theory in advancing our understanding of material science and chemistry.

## Results and Discussion

The study delves deeply into the intricate interactions between BP and  $C_8B_6N_6$  (a boron-nitrogen-carbon compound) by meticulously examining three distinct spatial configurations to determine the most energetically favorable arrangement. Each configuration represents a unique orientation of the two molecules, shedding light on their potential interactions and structural adaptations. In the first arrangement, referred to as the A-configuration, the  $C_8B_6N_6$  molecule is strategically aligned parallel to the benzene ring of BP, facilitating  $\pi$ - $\pi$  stacking interactions. The second arrangement, known as the B-configuration, involves positioning  $C_8B_6N_6$  in close proximity to the carbonyl group of BP, which is a highly electronegative functional group capable of engaging in dipole-dipole or hydrogen bonding interactions. The third and final arrangement, termed the C-configuration, places the  $C_8B_6N_6$  molecule near the alkyl chain of BP, an area that could potentially allow for Van der Waals forces or other non-covalent interactions to occur. After performing comprehensive geometrical optimization, as illustrated in Figure 2, it was observed that in all three configurations, BP exhibited a pronounced tendency to move

closer to the  $C_8B_6N_6$  molecule. This convergence resulted in notable structural modifications in both molecules, indicating a significant level of interaction between them. The observed structural changes underscore the strength and nature of the intermolecular forces at play, which appear to be robust across all configurations. These findings, supported by prior research [25], highlight the strong affinity between BP and  $C_8B_6N_6$ , providing valuable insights into their interaction dynamics and potential applications in fields such as material science or molecular engineering.

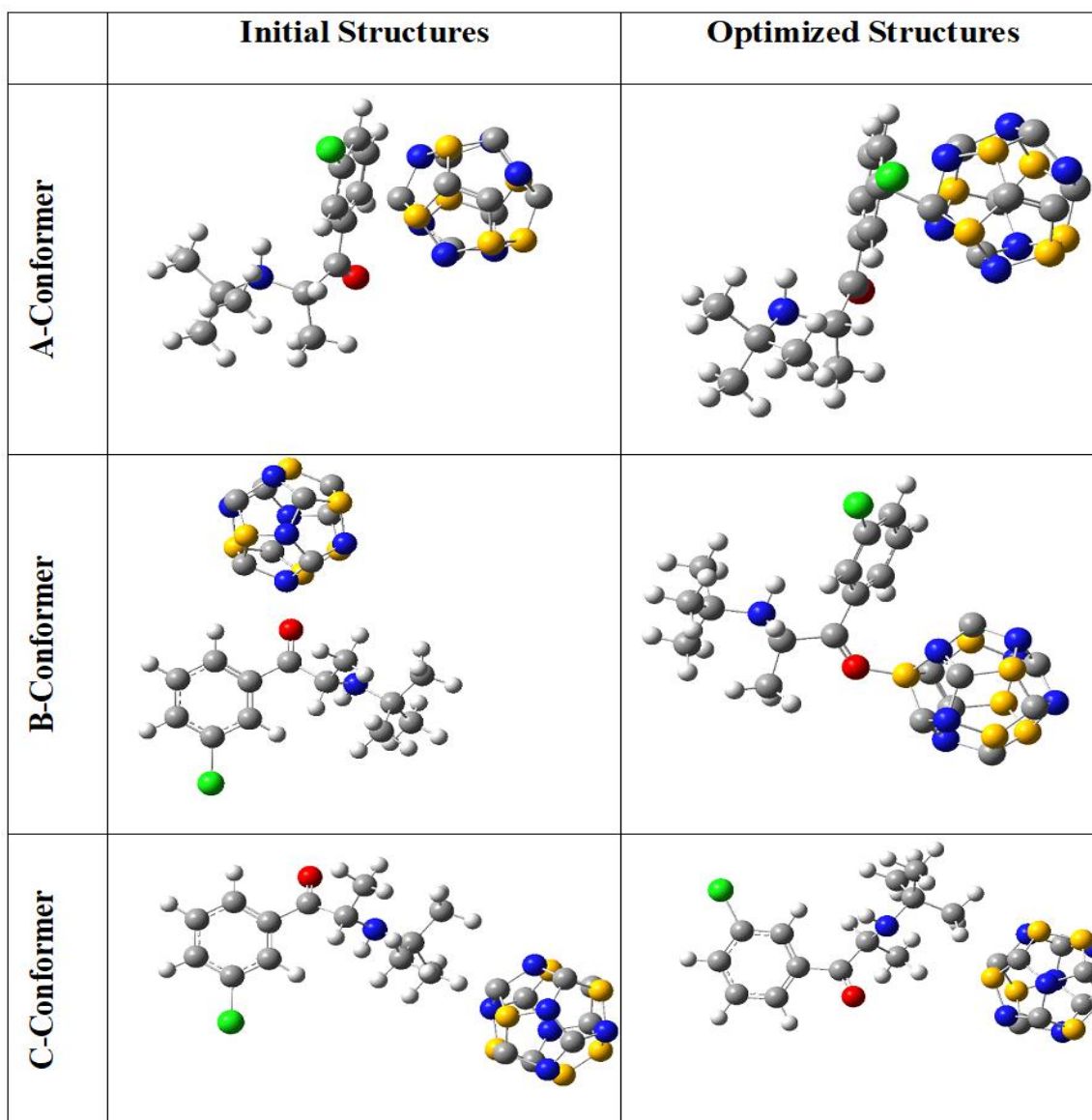


**Figure 2.** The initial and optimized structures of BP and  $C_8B_6N_6$  complexes (grey: carbon, white: hydrogen, red: oxygen, blue: nitrogen, yellow: boron, green: chlorine)

The data presented in Table 1 highlights critical insights into the thermodynamics and stability of the adsorption process under experimental conditions. Notably, the adsorption energies reported are negative across all configurations examined, signifying that these processes are thermodynamically favorable. Among the various configurations studied, the A-Conformer emerges as the most energetically favorable, exhibiting the most negative adsorption energy. This observation underscores the particularly strong interactions associated with this conformer, as previously established in the literature [24]. Furthermore, the influence of water as a solvent on these adsorption energies was systematically investigated. The findings reveal that the presence of water leads to a slight increase in adsorption energies [23], suggesting a minor weakening of interactions in an aqueous medium. Despite this, the adsorption process remains feasible under experimental conditions, demonstrating that water's role as a solvent only marginally affects the overall thermodynamics of adsorption [25].

**Table 1.** Structural properties of BP, C<sub>8</sub>B<sub>6</sub>N<sub>6</sub>, and their complexes

Structures	Adsorption energy (kJ/mol)	$\nu_{\min}$ (cm <sup>-1</sup> )	$\nu_{\max}$ (cm <sup>-1</sup> )	Dipole moment (Deby)
BP (Vacuum)	---	15.755	3220.933	1.920
BP (Water)	---	25.340	3223.904	2.140
C <sub>8</sub> B <sub>6</sub> N <sub>6</sub> (Vacuum)	---	55.754	2163.132	0.770
C <sub>8</sub> B <sub>6</sub> N <sub>6</sub> (Water)	---	70.766	2153.209	0.980
A-Conformer (Vacuum)	-145.019	10.365	4006.343	5.440
A-Conformer (Water)	-65.380	15.139	3878.436	6.120
B-Conformer (Vacuum)	-98.519	23.534	3883.021	12.650
B-Conformer (Water)	-57.256	20.305	3953.153	13.310
C-Conformer (Vacuum)	-77.278	20.933	3733.055	3.160
C-Conformer (Water)	-43.457	22.431	3812.216	4.090

To further validate the stability of the adsorbed structures, geometrical optimization was performed, followed by infrared (IR) spectral calculations. The results of these calculations, as summarized in Table 1, consistently show positive minimum and maximum frequency values for all structures analyzed. These positive frequency values confirm that the optimized geometries correspond to true local minima on the potential energy surface, thereby affirming their structural stability. This finding not only validates the robustness of the computational methods employed

but also highlights their reliability in advancing theoretical predictions and practical applications in related chemical systems [22]. Such robust computational approaches are indispensable for understanding complex adsorption phenomena and for designing materials with tailored properties. Additionally, Table 1 provides valuable data on changes in dipole moment resulting from the interaction between BP (the adsorbate) and the  $C_8B_6N_6$  nanocage (the adsorbent). These changes in dipole moment are particularly noteworthy, as they suggest a significant enhancement in BP's chemical reactivity upon adsorption. The observed variations in dipole moment are indicative of substantial shifts in electronic distribution and charge transfer within the BP-adsorbent complex. This phenomenon provides deeper insights into the electronic behavior of the system, shedding light on how such interactions can influence the chemical and electronic properties of both the adsorbate and the adsorbent [21]. Collectively, these findings contribute to a more comprehensive understanding of adsorption processes and their implications for material design and chemical reactivity.

The thermodynamic analysis presented in Table 2 provides compelling evidence that the interaction between BP and  $C_8B_6N_6$  is not only highly exothermic but also occurs spontaneously, requiring no external energy input to drive the process [22]. This conclusion is substantiated by the consistently negative values observed for both the enthalpy change ( $\Delta H_{ad}$ ) and Gibbs free energy change ( $\Delta G_{ad}$ ), which are hallmark indicators of a thermodynamically favorable reaction. Furthermore, the substantial thermodynamic equilibrium constants lend additional support to these findings, reinforcing the robustness of the observed phenomena [18]. The study delves deeper into the influence of external factors, such as temperature and solvent environments, on these thermodynamic parameters. Results indicate that BP adsorption achieves optimal efficiency under lower temperature conditions and within a vacuum setting, highlighting the sensitivity of the process to environmental variables [17]. However, the negative entropy change ( $\Delta S_{ad}$ ) values associated with the adsorption process suggest an entropically unfavorable mechanism. This observation implies a tendency for BP molecules and adsorbent clusters to aggregate post-adsorption, reflecting a reduction in system disorder [20]. Interestingly, the thermodynamic data also reveal a distinct preference for the A-Conformer configuration over other conformers, suggesting structural advantages that enhance interaction stability. Despite these favorable attributes, the relatively low equilibrium constant values point to an inherent reversibility in the interactions between BP and  $C_8B_6N_6$ . This reversibility indicates that the

adsorption process proceeds bidirectionally and adheres to equilibrium dynamics, allowing for the possibility of desorption under certain conditions [21]. Collectively, these findings provide a nuanced understanding of the thermodynamic behavior governing BP adsorption and offer valuable insights into how external factors and molecular conformations influence the efficiency and stability of this process.

**Table 2.** Thermodynamic parameters of the adsorption process as a function of temperature

Structures	$\Delta H_{ad}$ (kJ/mol)	$\Delta G_{ad}$ (kJ/mol)	$\Delta S_{ad}$ (J/mol)	$K_{th}$
<b>A-Conformer-Vacuum-298</b>	-149.623	-84.965	-33.134	$7.692 \times 10^{+14}$
<b>A-Conformer-Vacuum-308</b>	-147.823	-82.660	-35.694	$1.029 \times 10^{+14}$
<b>A-Conformer-Vacuum-318</b>	-146.023	-80.355	-38.254	$1.561 \times 10^{+13}$
<b>A-Conformer-Water-298</b>	-83.739	-19.080	-15.125	$2.202 \times 10^{+03}$
<b>A-Conformer-Water-308</b>	-81.939	-16.775	-17.335	$6.976 \times 10^{+02}$
<b>A-Conformer-Water-318</b>	-80.139	-14.470	-19.315	$2.376 \times 10^{+02}$
<b>B-Conformer-Vacuum-298</b>	-95.669	-50.655	-15.903	$7.496 \times 10^{+08}$
<b>B-Conformer-Vacuum-308</b>	-93.869	-48.350	-18.354	$1.571 \times 10^{+08}$
<b>B-Conformer-Vacuum-318</b>	-92.069	-46.045	-19.572	$3.631 \times 10^{+07}$
<b>B-Conformer-Water-298</b>	-62.035	-17.021	-28.076	$9.596 \times 10^{+02}$
<b>B-Conformer-Water-308</b>	-60.235	-14.716	-29.925	$3.123 \times 10^{+02}$
<b>B-Conformer-Water-318</b>	-58.435	-12.411	-30.498	$1.091 \times 10^{+02}$
<b>C-Conformer-Vacuum-298</b>	-91.120	-46.106	-82.294	$1.196 \times 10^{+08}$
<b>C-Conformer-Vacuum-308</b>	-89.320	-43.801	-84.124	$2.660 \times 10^{+07}$
<b>C-Conformer-Vacuum-318</b>	-87.520	-41.496	-86.893	$6.503 \times 10^{+06}$
<b>C-Conformer-Water-298</b>	-61.780	-16.766	-52.954	$8.658 \times 10^{+02}$
<b>C-Conformer-Water-308</b>	-59.980	-14.461	-54.784	$2.827 \times 10^{+02}$
<b>C-Conformer-Water-318</b>	-58.180	-12.156	-57.553	$9.905 \times 10^{+01}$

The comprehensive analysis of the density of states (DOS) spectra and the frontier molecular orbital (FMO) parameters, as presented in Table 3 and Figure 3, reveals noteworthy alterations in the electronic properties of  $C_8B_6N_6$  when subjected to adsorption. A particularly striking observation is the significant reduction in the band gap of  $C_8B_6N_6$ , which initially measured at 2.380 eV. Upon adsorption, this band gap undergoes substantial decreases, reaching values of 1.922 eV, 1.144 eV, and 2.317 eV for conformers A, B, and C, respectively. Among these, the B-Conformer exhibits the most pronounced shift, with a remarkable reduction of approximately 52%, highlighting its unique electronic adaptability. These findings underscore the immense potential of  $C_8B_6N_6$  as a highly effective electrocatalyst modifier, particularly in applications related to BP detection [24].

**Table 3.** FMO parameters for BP,  $C_8B_6N_6$ , and their complexes

Structures	$E_{HOMO}$ (eV)	$E_{LUMO}$ (eV)	$E_g$ (eV)	% $\Delta E_g$	$\eta$ (eV)	$\mu$ (eV)	$\omega$ (eV)	$\Delta N_{max}$ (eV)
BP	-6.476	-2.099	4.378	---	2.189	-4.288	4.199	1.959
$C_8B_6N_6$	-5.909	-3.529	2.380	---	1.190	-4.719	9.358	3.966
A-Conformer	-6.217	-4.296	1.922	-19.253	0.961	-5.256	14.379	5.471
B-Conformer	-4.781	-3.637	1.144	-51.940	0.572	-4.209	15.492	7.361
C-Conformer	-5.743	-3.426	2.317	-2.644	1.158	-4.584	9.071	3.957

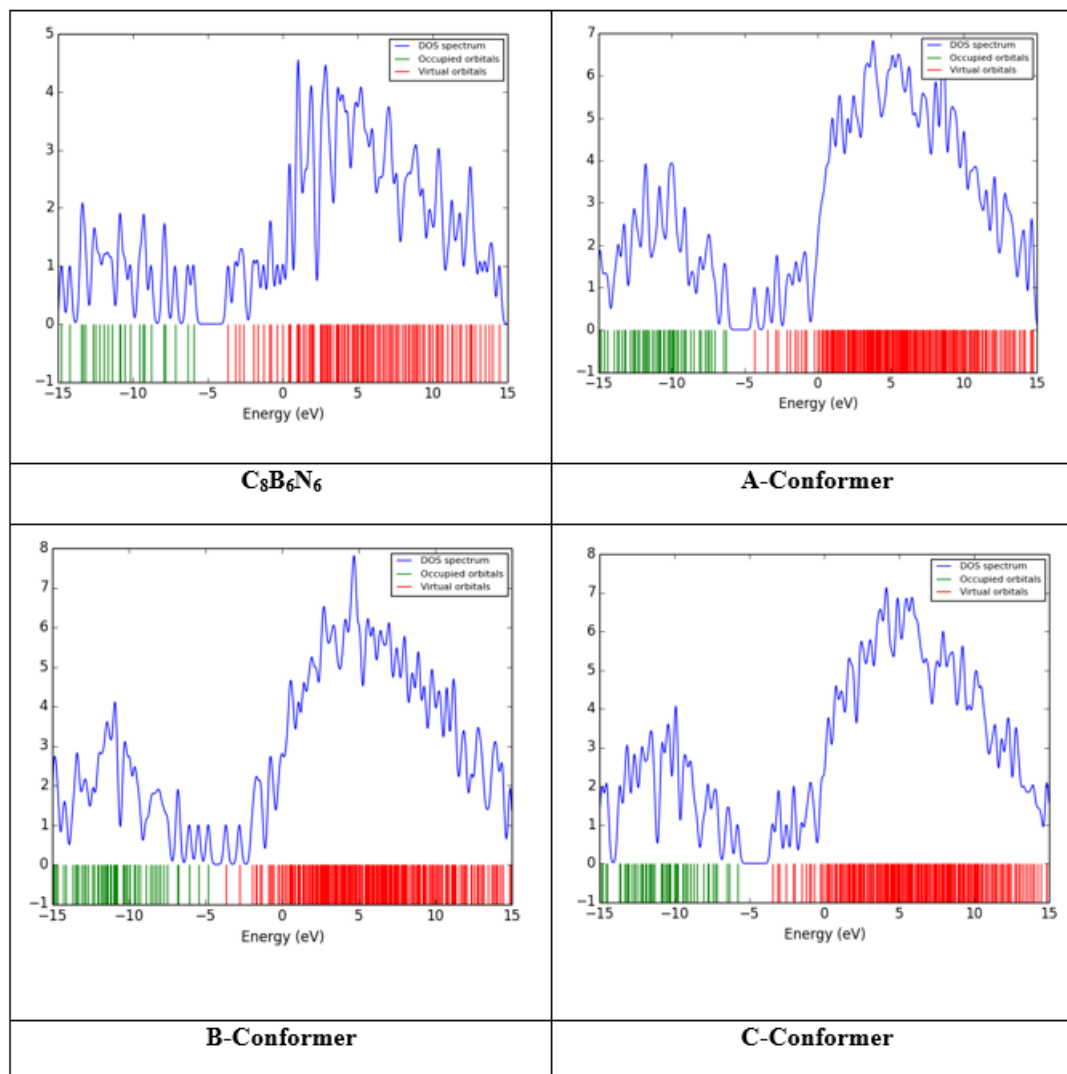


**Figure 3.** The DOS spectrums of BP and C<sub>8</sub>B<sub>6</sub>N<sub>6</sub> complexes

Beyond the changes in band gap, adsorption also induces a notable reduction in the chemical hardness of BP. Initially recorded at 2.189 eV, the chemical hardness decreases significantly to 0.961 eV, 0.572 eV, and 1.158 eV for conformers A, B, and C, respectively. This reduction in chemical hardness is indicative of an enhancement in the chemical reactivity of BP following its interaction with C<sub>8</sub>B<sub>6</sub>N<sub>6</sub> [25]. These changes suggest that the adsorption process facilitates a more reactive chemical environment, which could be advantageous for catalytic or sensing applications. Furthermore, the observed negative values of chemical potential for all configurations provide strong evidence of their thermodynamic stability, reinforcing the viability of these systems under experimental conditions. Additionally, adsorption on the C<sub>8</sub>B<sub>6</sub>N<sub>6</sub> surface

leads to significant improvements in both the electrophilicity index and the maximum charge transfer capacity of BP. These enhanced properties suggest a greater ability of the BP molecules to accept electrons when interacting with the nanostructured surface of  $C_8B_6N_6$  compared to their isolated counterparts. This increased electron-accepting capability further emphasizes the critical role of nanostructural interactions in modulating the electronic characteristics of molecular systems [23]. Collectively, these findings not only highlight the transformative impact of adsorption on the electronic and chemical properties of BP but also establish  $C_8B_6N_6$  as a promising material for advanced applications in electrocatalysis and molecular detection technologies.

## Conclusion

This research delved into the potential of the  $C_8B_6N_6$  nanocluster as an advanced adsorbent and sensor for the removal and detection of bupropion (BP), leveraging density functional theory (DFT) methodologies. The study meticulously analyzed the interaction dynamics between BP and the  $C_8B_6N_6$  nanocage, revealing that the adsorption process is not only experimentally viable but also characterized by a reversible semi-chemisorption nature. Thermodynamic evaluations provided compelling evidence for the exothermic and spontaneous nature of this adsorption, as indicated by the negative values of enthalpy change ( $\Delta H_{ad}$ ) and Gibbs free energy change ( $\Delta G_{ad}$ ). Furthermore, the influence of environmental factors such as temperature and solvent presence was examined, demonstrating that adsorption efficiency is enhanced at lower temperatures and in the absence of water, particularly within the gas phase. In addition to its adsorption properties, the nanocage exhibited notable alterations in its electronic structure upon interaction with BP. Specifically, a substantial 52% reduction in its bandgap was observed, with the value decreasing from 2.380 eV to 1.144 eV. This pronounced change underscores the nanocluster's dual functionality, not only as a highly effective material for BP removal but also as an excellent candidate for sensing applications, particularly in electrochemical detection systems. The findings from this study highlight the versatile capabilities of the  $C_8B_6N_6$  nanocluster and its promising role in environmental remediation and analytical sensing technologies.

## References

[1] J. Akhtar, N.A. Amin, K. Shahzad, *Desalination Water Treat.*, 57, 12842 (2016).

- [2] L. Huang, R. Shen, Q. Shuai, *Environ. Manag.*, 277, 111389 (2021).
- [3] A. Thakur, A. Kumar, A. Singh, *Carbon*, 217, 118621 (2024).
- [4] S. Jiang, Y. Lyu, J. Zhang, X. Zhang, M. Yuan, Z. Zhang, G. Jin, B. He, W. Xiong, Yi H., *J. Environ. Chem. Eng.*, 12, 111951 (2024).
- [5] M.E. Peñafiel, L. Jara-Cobos, D. Flores, C. Jerves, M. Menendez, *Case Stud. Chem. Environ. Eng.*, 9, 100575 (2024).
- [6] G. Lee, I. Ahmed, H.J. Lee, S.H. Jung, *Sep. Purif. Technol.*, 20, 127602 (2024).
- [7] Z. NazarAli, S.A. Ahmadi, D. Ghazanfari, E. Sheikhhosseini, *Nanochem Res.*, 7, 22 (2022).
- [8] S. Kurumoglu, Y.Y. Gurkan, *Bulg. Chem. Commun.*, 55, 299 (2023).
- [9] E. Maccaroni, L. Malpezzi, A. Famulari, N. Masciocchi, *J Pharm Biomed Anal.*, 60, 65 (2012).
- [10] S. Jafari, M. Dehghani, N. Nasirizadeh, M. Azimzadeh, F.D. Banadaki, *Bull. Mater. Sci.*, 44, 56 (2021).
- [11] M. Madej, A. Trzcińska, J. Lipińska, R. Kapica, M. Fronczak, R. Porada, J. Kochana, B. Baś, J. Tyczkowski, *Mikrochim. Acta*, 190, 391 (2023).
- [12] S.E. Algmaal, A.M. Mahmoud, S.A. Boltia, Y.S. El-Saharty, N.S. Ghoniem, *Sci. Rep.*, 14, 29305 (2024).
- [13] M.R. Ganjali, F. Mizani, P. Norouzi, *Int. J. Electrochem. Sci.*, 7, 7631 (2012).
- [14] R. Saini, S.A. Doi, K.K. Jhankal, D.K. Sharma, *Chem Sci Trans.*, 6, 330 (2017).
- [15] A. Koltsakidou, K.N. Maroulas, E. Evgenidou, D.N. Bikiaris, G.Z. Kyzas, D.A. Lambropoulou, *J. Mol. Liq.*, 12, 127147 (2025).
- [16] E. Evgenidou, A. Rapti, L.A. Koronaiou, S. Petromelidou, K. Anagnostopoulou, D. Lambropoulou, *SCENV.*, 3, 100028 (2023).
- [17] P. Niknam Rad, M. Qomi, M.R. Jalali Sarvestani, *J. Nanomed. Res.*, 9, 206 (2024).

- [18] A. Behnia, M.R. Jalali Sarvestani, A. Abdulmutaleb Ibrahim, M.S. Mahdi, *Chem. Rev. Lett.*, 7, 993 (2024).
- [19] M. Yousefi, M.S. Rad, R. Shakibazadeh, L. Ghodrati, M.A. Kachoie, *Mol Simul.*, 48, 1284 (2022).
- [20] T. Yadav, E. Shakerzadeh, S. Goswami, E. Tahmasebi, J. Adam, S. Garai, *Diam. Relat. Mater.*, 149, 111600 (2024).
- [21] R. Di Felice, A. Selloni, E. Molinari, *J. Phys Chem. B*, 107, 1151 (2002).
- [22] K. Nakada, A. Ishii, *Graphene Simulation*. IntechOpen, (2003).
- [23] B. Zhu, L. Zhang, D. Xu, B. Cheng, J. Yu, *J CO<sub>2</sub> UTIL.*, 21, 327 (2017).
- [24] A.S. Rad, K. Ayub, *J. Alloys Compd.*, 678, 317 (2016).
- [25] F. Azarakhshi, S. Shahab, S. Kaviani, M. Sheikhi, *Lett. Org. Chem*, 18, 640 (2021).
- [26] R. Dennington, T.A. Keith, J.M. Millam, GaussView, Version 6.1, Semichem Inc., Shawnee Mission, KS, (2016).
- [27] S. Melchor, J.A. Dobado, *Chem. Inf. Comput. Sci.*, 44, 1639 (2004).
- [28] M. J. Frisch, G. W. Trucks, H. B. Schlegel, G. E. Scuseria, M. A. Robb, J. R. Cheeseman, G. Scalmani, V. Barone, G. A. Petersson, H. Nakatsuji, X. Li, M. Caricato, A. V. Marenich, J. Bloino, B. G. Janesko, R. Gomperts, B. Mennucci, H. P. Hratchian, J. V. Ortiz, A. F. Izmaylov, J. L. Sonnenberg, D. Williams-Young, F. Ding, F. Lipparini, F. Egidi, J. Goings, B. Peng, A. Petrone, T. Henderson, D. Ranasinghe, V. G. Zakrzewski, J. Gao, N. Rega, G. Zheng, W. Liang, M. Hada, M. Ehara, K. Toyota, R. Fukuda, J. Hasegawa, M. Ishida, T. Nakajima, Y. Honda, O. Kitao, H. Nakai, T. Vreven, K. Throssell, J. A. Montgomery, Jr., J. E. Peralta, F. Ogliaro, M. J. Bearpark, J. J. Heyd, E. N. Brothers, K. N. Kudin, V. N. Staroverov, T. A. Keith, R. Kobayashi, J. Normand, K. Raghavachari, A. P. Rendell, J. C. Burant, S. S. Iyengar, J. Tomasi, M. Cossi, J. M. Millam, M. Klene, C. Adamo, R. Cammi, J. W. Ochterski, R. L. Martin, K. Morokuma, O. Farkas, J. B. Foresman, and D. J. Fox, Gaussian 16, Revision C.01, Gaussian, Inc., Wallingford CT, 2016, GaussView 5.0. Wallingford, E.U.A.

[29] M. Orio, D.A. Pantazis, F. Neese, *Photosynth. Res.*, 102, 443 (2009).

[30] M. Stahn M., S. Ehlert, S. Grimme, *J. Phys. Chem. A*, 127, 7036 (2023).

#### HOW TO CITE THIS ARTICLE

Mohammad Hossein Razeghi, Ozra Gholipour, Simin Arabi, Ebrahim Nemati-Kande, Jaber Jahanbin Sardroodi, “**A DFT Outlook on Bupropion Adsorption on the Surface of C<sub>8</sub>B<sub>6</sub>N<sub>6</sub> Nanocluster**” *International Journal of New Chemistry.*, 2025; 11(4), 903-921.